Transient Kinetics and Mechanics of Myosin's Force-Generating Rotation in Muscle: Resolution of Millisecond Rotational Transitions in the Spin-Labeled Myosin Light-Chain Domain†

Leslie E. W. LaConte, Josh E. Baker,‡ and David D. Thomas*

Department of Biochemistry, Molecular Biology and Biophysics, University of Minnesota, Minneapolis, Minnesota 55455

Received February 20, 2003; Revised Manuscript Received May 30, 2003

ABSTRACT: We have used electron paramagnetic resonance (EPR) of spin-labeled scallop muscle, in conjunction with laser flash photolysis of caged ATP, to resolve millisecond rotational transitions of the myosin light-chain domain (LCD) during transient force generation. We previously used EPR to resolve two distinct orientations of the LCD [Baker, J. E., Brust-Mascher, I., Ramachandran, S., LaConte, L. E., and Thomas, D. D. (1998) *Proc. Natl. Acad. Sci. U.S.A. 95*, 2944−2949], correlated these structural states with biochemical states in the actin−myosin ATPase reaction, and showed that a small shift in the steady-state distribution between these two LCD orientations (i.e., a net lever arm rotation) is associated with force generation in muscle. In the study presented here, we measured millisecond changes in this orientational distribution (i.e., the rates of transition between the two LCD orientations) in muscle following flash photolysis of caged ATP, in both the presence and absence of Ca. The transient acquired in the absence of Ca is dominated by a rapid ($1/\tau_1 = 37\ s^{-1}$) disordering transition from the single orientation in rigor to the bimodal orientation distribution observed for detached cross-bridges in relaxation (i.e., the reversal of the lever arm rotation), followed by a recovery phase ($1/\tau_2 = 2.4\ s^{-1}$) of very small amplitude (small fraction of heads participating). In the presence of Ca, the transient exhibited a similar initial disordering phase ($1/\tau_1 = 38.5\ s^{-1}$), followed by a recovery phase ($1/\tau_2 = 8.33\ s^{-1}$) of substantial amplitude, corresponding to the forward rotation and ordering of the lever arm. A standard kinetic model was used to fit these data, revealing rate constants consistent with those previously determined by other methods. Surprisingly, a comparison of the EPR transients with force transients reveals that the rate of force development ($91\ s^{-1}$) is faster than the rate of the forward lever arm rotation ($8\ s^{-1}$). This observed relationship between the kinetics of the lever arm rotation and transient force development in muscle provides new insight into how myosin both generates and responds to muscle force.

The goal of muscle research for the past 20 years has been to identify the molecular mechanism responsible for force generation. The proposal that the light-chain domain of myosin II in muscle fibers rotates upon activation to serve as a lever arm (*2*) has much experimental support (*1*, *3*−*5*). An electron paramagnetic resonance (EPR)[1] sensitive spectroscopic probe (spin label), attached to the regulatory light chain (RLC) of myosin, has been shown to rotate approximately 36° upon activation of muscle fibers (*1*). This LCD rotation, corresponding to a myosin biochemical transition from a weak to a strong actin-binding state, appears to be the major molecular movement responsible for force development in muscle (*6*).

The relationship between myosin mechanics and muscle mechanics has previously been inferred from comparisons of actin−myosin ATPase kinetics and force transients in muscle. These studies provide the basis for most current muscle contraction models (*7*, *8*). The spin-labeled muscle fiber system used to describe the 36° light-chain domain rotation provides an exciting opportunity to directly correlate myosin structural rearrangements with a change in muscle force, by simultaneously measuring EPR and muscle mechanics transients. These measurements provide a direct link between the molecular mechanisms of force generation, myosin ATPase kinetics, and force generation kinetics.

These kinetics experiments employ the technology of the rapid release of caged ATP (*9*−*11*) throughout the muscle fiber lattice with a burst of laser light. A typical experiment begins with a muscle fiber in the rigor state in the presence of 10 mM caged ATP, with essentially all myosin heads bound strongly to actin. Upon laser flash-induced photolysis of caged ATP (c-ATP), ATP is released and causes the muscle fiber to relax (in the absence of Ca) or to generate force (in the presence of Ca). EPR provides a linear readout of resolved structural states, so when a single point in the EPR spectrum is monitored for changes after photolysis, the

† This work was supported by grants to D.D.T. from the National Institutes of Health (AR32961), the Muscular Dystrophy Association, and the Minnesota Supercomputing Institute. L.E.W.L. was supported by predoctoral training grants from the National Institutes of Health (T32 GM 08277 and AR07612) and a Doctoral Dissertation Fellowship from the University of Minnesota Graduate School.

* To whom correspondence should be addressed. Phone: (612) 625-0957. Fax: (612) 624-0632. E-mail: ddt@ddt.biochem.umn.edu.

‡ Current address: Department of Molecular Physiology and Biophysics, University of Vermont, Burlington, VT 05405-0068.

[1] Abbreviations: EPR, electron paramagnetic spectroscopy; LCD, light-chain domain; RLC, regulatory light chain; FDNASL, 3-(5-fluoro-2,4-dinitroanilino)-2,2,5,5-tetramethyl-1-pyrrolidinyloxy spin label; c-ATP, caged ATP {P^3-[1-(2-nitrophenyl)ethyl]adenosine 5′-triphosphate}.

10.1021/bi034288r CCC: $25.00
Published on Web 07/24/2003

rate of this change provides a measurement of the rate of structural transitions during relaxation or contraction. These rates can then be compared to previously measured rates for steps in the myosin ATPase cycle for a more accurate description of how myosin structure, biochemistry, and force generation are linked in muscle.

It has been shown previously (*6*) that the EPR spectrum of the weak-binding myosin structure contains two orientational components that correspond to the splayed heads of the myosin dimer (*5*, *12*, *13*), suggesting that the ATP-induced transition from the strong-binding to weak-binding structure (not the ATP hydrolysis step) is the mechanism for the reversal of the lever arm rotation. In the study presented here, we report the time course of the reverse lever arm rotation and compare this transient structural transition to the kinetics of ATP-induced actin−myosin detachment. EPR transients following Ca activation of the muscle fibers reveal the forward lever arm rotation rate. This experimental system provides the opportunity to simultaneously monitor myosin structural changes and force generation. A comparison of the rates of force development and the redistribution of myosin weak- and strong-binding states (rotation of the light-chain domain) yields intriguing results about changes in the force borne per myosin head during force development. Our kinetic data are discussed in terms of a previously described two-state model of muscle contraction (*14*).

MATERIALS AND METHODS

RLC Purification and Labeling. RLCs were purified from chicken gizzard myosin (*15*) and spin-labeled with the 3-(5-fluoro-2,4-dinitroanilino)-2,2,5,5-tetramethyl-1-pyrrolidinyloxy spin label (FDNASL) by incubating 40 μM RLC with 100 μM FDNASL (pH 7 and 4 °C) for 20 h. The spin/protein ratio was 0.9 ± 0.1, indicating complete and specific reaction with the single thiol on Cys108.

Scallop Fiber Preparation and RLC Exchange. Fiber bundles were prepared from scallop (*Placopecten magellanicus*) adductor muscle (*16*) without Triton treatment. Bundles of 0.4−1.0 mm were dissected either from fresh tissue (all mechanical experiments) or from bundles of tissue that were stored at −20 °C in 50% glycerol and 50% buffer A [40 mM NaCl, 0.1 mM NaN_3, and 10 mM MOPS (pH 7)] with 2 mM $MgCl_2$. Dissected bundles approximately 25 mm in length and 0.2 mm in diameter were tied on both ends with surgical silk thread to hold them isometrically and then put in borosilicate capillary tubes with an inner diameter of 1.0 mm and an outer diameter of 1.5 mm. Extraction of native RLC and addition of chicken gizzard RLC were performed as described previously (*6*).

Fiber Mounting. For experiments in the TM cavity, three to four exchanged bundles were trimmed to 10 mm in length, tied together, and threaded through a single borosilicate capillary tube. These bundles could then be monitored for force changes during the experiment. For experiments in the TE cavity, three to four exchanged bundles were secured to a Kel-F flat cell cover plate. The cover plate (10 mm × 4 mm) had a well with a depth of 1 mm (volume of 25 μL) in which eight pairs of holes were drilled. Surgical silk thread was threaded through these holes to form a series of loops down the long edges of the well. Fibers were threaded underneath these loops, the loops were pulled taut, and the fibers were trimmed to span the well. The cover plate was secured to a quartz-Suprasil flat cell (WG-807, Wilmad) using vacuum grease.

Force Measurements. Isometric force was measured simultaneously during EPR spectrum acquisition as described previously (*6*) with slight modification. The thread on the end of the bundle opposite the strain gauge was threaded into a chamber and through a hole in a brass bar. The thread was secured to the bar with Devcon Duco Cement. This bar could then be turned to adjust the starting tension of the fiber. The chamber was then closed with a seal containing a small hole through which solution was continuously flowed over the fibers using a LKB Microperpex (Bromma, Sweden) peristaltic pump at a rate of 0.2 mL/min.

Force data sets were collected using a LabView (National Instruments, Austin, TX) program written by R. Loegering. In force traces accompanying steady-state EPR spectra, 128 data points/s were acquired and then averaged into a single point plotted each second. In force traces accompanying transient EPR spectra, 10 000 data points/s were acquired and then averaged so that 1000 points were plotted every second (1 ms time constant).

Activation of Fibers by Photolysis of c-ATP. Transient experiments were initiated by a single 10 ns pulse of 351 nm light from a XeF excimer laser (LPX200i; Lambda Physik, Acton, MA) focused directly into the optical port of the TE cavity or through a single slit in the optical grating of the TMA cavity. The light was focused such that the entire sample was uniformly exposed. Prior to activation, the fibers were washed first with rigor buffer and then relaxation buffer and then returned to rigor buffer. A caged ATP solution was then added. A LabView (National Instruments) program written by J. Grinband controlled the initiation of laser firing and EPR acquisition.

EPR Spectroscopy and Analysis. EPR spectra were acquired on a Bruker EleXsys 500 X-band spectrometer. Steady-state EPR spectra were obtained in the conventional manner, sweeping the magnetic field through 120 G with a time constant and conversion time of 40 ms, with four scans per spectrum. Transient data sets were acquired by selecting a single field position (the low-field peak, termed M2 at ∼3442 G, of the muscle fiber spectrum in rigor, Figure 1) and acquiring intensity changes at this field position over a period of 1 s, with a time constant and conversion time of 5 ms. A digital "gate" (constructed by R. Bennett) was placed in front of the spectrometer signal channel to eliminate a sharp (∼10 ns) signal artifact due to the laser pulse and photolysis of c-ATP. It has been shown previously that EPR spectra in this system are a linear combination of two spectral components corresponding to distinct *orientational states* (M1 and M2) of the myosin *head* (light-chain domain), differing in axial orientation by 30−40° (*1*, *6*). That is, at every field position, the EPR spectrum is given by $V = x_1V_1 + x_2V_2$, where x_i is the mole fraction. Those studies also showed that the spectrum is a linear combination of two *structural states* of the two-headed myosin *molecule*: $V = x_SV_S + x_WV_S$, where x_S is the fraction of molecules in the strong-binding state, in which both heads have the M2 orientation, and x_W is the fraction of molecules in the weak-binding state, in which one head has the M2 orientation and the other has the M1 orientation. Since $x_1 + x_2 = x_S + x_W = 1$, $x_2 = 0.5 + 0.5x_S$ and $x_S = 2x_2 - 1$. Thus, the EPR

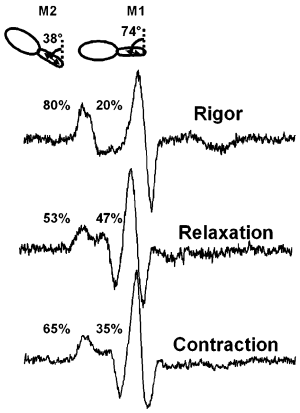

FIGURE 1: Steady-state EPR spectra of scallop muscle fibers labeled with FDNASL on Cys108 of the RLC (*6*). Fibers were aligned parallel to the magnetic field. M1 is the structural component that is more populated in weak-binding states. This state has an EPR spectrum indicating that the principal axis of the rigidly bound nitroxide spin label is oriented at 38° with respect to the muscle fiber backbone (aligned with the magnetic field). M2 is the strong-binding state, in which the probe is oriented at 74°. The percentage of heads in each structural state is indicated.

Scheme 1: Actomyosin ATPase Kinetic Cycle Used To Analyze Transient Data

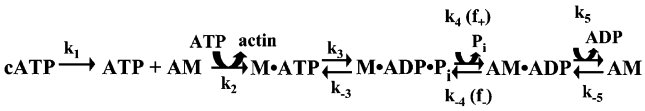

transient $V(t)$ at any spectral position is proportional to both $x_2(t)$ and $x_S(t)$.

Exponential Fits of Transient Data. Exponential fits and data smoothing were performed in Microcal Origin 6.0. Individual relaxation and contraction transients were averaged and smoothed with an 11-point Savitzky−Golay filter, and then the first 2 s of each transient was fit to the following equation using the Levenberg−Marquardt algorithm:

$$Y = (A_1 - c)e^{-t/\tau_1} + A_2(1 - e^{-t/\tau_2}) + c \qquad (1)$$

Kinetic Modeling of Transient Data. Kinetic modeling of the transient traces was done using the program Gepasi 3 (*17*−*19*). The data were fit to a five-step kinetic mechanism (Scheme 1), constrained by literature values as discussed in Results. Each step was defined using the mass action kinetic type; all steps except for the first were considered reversible. The EPR signal was assumed to be proportional to the mole fraction x_S of myosin molecules in the strong-binding AM·D and AM states, and it was the change in this parameter over time that was fit using the Levenberg−Marquardt method, with a stopping criterion of 10^{-5}. (The fitting procedure stops when the relative change in the objective function and the average relative change in the adjustable parameter values are both smaller than this value.)

Reagents and Solutions. Rigor buffer contained 20 mM MOPS, 5 mM $MgCl_2$, 1 mM EGTA, and 0.1 mM NaN_3. Relaxation and contraction buffers contained, in addition, 5 mM ATP, 20 mM creatine phosphate, and 0.25 mg/mL creatine phosphokinase; the contraction buffer had a pCa of 4.0. Caged ATP buffers contained 20 mM MOPS, 15 mM $MgCl_2$, 1 mM EGTA, 20 mM creatine phosphate, 0.25 mg/mL creatine phosphokinase, 10 mM glutathione (to protect fibers from free radical damage), and 10 mM c-ATP; c-ATP contraction buffer had a pCa of 4.0. The ionic strength of all buffers was adjusted to 200 mM with potassium propionate. Creatine phosphokinase was supplied by Boehringer-Mannheim. Caged ATP {P^3-[1-(2-nitrophenyl)-ethyl]adenosine 5′-triphosphate, disodium salt} was supplied by CalBiochem. All other reagents were supplied by Sigma.

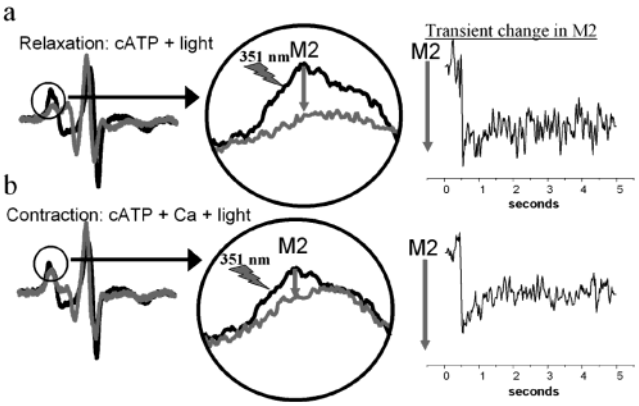

FIGURE 2: Single-field position monitored in an effort to capture the transient shift in population. (a) The muscle fiber begins in the state of rigor (black spectrum) in the presence of c-ATP. A flash of light causes the muscle fiber to relax (gray spectrum). The intensity of the circled peak decreases to the steady-state relaxation level (right side). (b) As in relaxation, except that Ca is present, resulting in contraction (black spectrum) upon release of c-ATP.

RESULTS

The design of these transient EPR experiments was based on steady-state EPR spectra previously described [Figure 1 (*1*, *6*)]. Analysis of spectra acquired from scallop muscle fibers containing a spin-labeled RLC revealed the constant presence of two spectral components, regardless of the physiological state of the fibers. The population distribution between these components is modulated by changing the physiological state of muscle (rigor, relaxation, and contraction). These spectral components correspond to two distinct orientations of the LC domain of myosin separated by approximately 36°. In rigor, most (>90%) of the LC domains occupy the M2 orientation (Figure 1), so M2 is the LC domain orientation induced by strong actin binding. Upon relaxation by addition of ATP, half of the LC domains rotate to occupy the M1 orientation, showing that when myosin is in the weak-binding state, the myosin dimer stabilizes a splayed head configuration (*5*, *12*, *13*). When Ca is added to initiate contraction, a small fraction of myosin LC domains (between 12 and 17%) rotate from the M1 to the M2 orientation, corroborating previous evidence that only a small fraction of heads is responsible for force generation (*1*, *20*).

By following the intensity of the spectral peak associated with strong actin binding (M2) upon release of caged ATP, we characterize the kinetics of the relaxation of the myosin dimer structure upon dissociation from actin (Figure 2). A single field position was identified, and intensity was monitored prior to, during, and following the laser flash that releases ATP from the chemical cage component surrounding the terminal phosphate group. Intensity changes occurred on the millisecond time scale. To capture the kinetics of the forward lever arm rotation associated with the strong-binding transition, Ca was added to the reaction mixture before

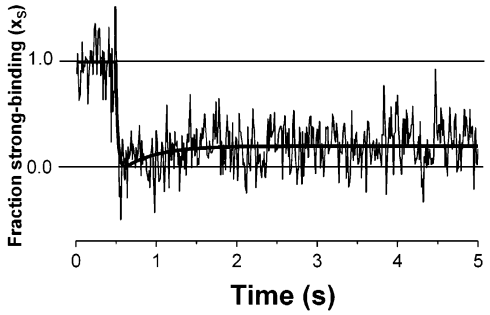

FIGURE 3: Transient rotation of spin-labeled RLC, induced by photolysis of caged ATP in the absence of Ca. The average of six transients is superimposed on the two-exponential fit.

photolysis. As shown in Figure 2, the signal intensity decreases upon photolysis of c-ATP in either the presence or absence of Ca, since the initial condition is rigor, in which most LC domains are in the M2 orientation. As explained in Materials and Methods, the vertical axis in the EPR transient is proportional to both x_2, the fraction of heads in the M2 orientation, and x_S, the fraction of myosin molecules in the strong-binding structural state.

Relaxation Transient. Upon photolysis of c-ATP in the absence of Ca, the EPR signal falls rapidly, indicating a complete depopulation of the strong-binding myosin structural state (50% depopulation of M2) within milliseconds (Figure 3). This is followed by a slower recovery phase with a much smaller amplitude. The biexponential fit gives a τ_1 of 0.027 ± 0.008 s^{-1} ($1/\tau_1 = 37 \pm 8$ s^{-1}) and a τ_2 of 0.41 ± 0.27 s^{-1} ($1/\tau_2 = 2.4 \pm 0.9$ s^{-1}). The rate of the rapid phase of this structural transient ($1/\tau_1 = 37 \pm 8.4$ s^{-1}) compares favorably to the rate of ATP binding and actin detachment, which is the biochemical step responsible for muscle relaxation. Previous measurements of the rate of scallop muscle fiber relaxation yield a value of 38.7 ± 3.4 s^{-1} (*21*), although a direct comparison cannot be made since this number was obtained by monitoring the tension decline following the release of a caged chelator that rapidly removes Ca from active scallop muscle fibers. Measurement of force transients during the release of cATP in the absence of Ca showed a large initial increase in force, followed by a decay to essentially zero force (data not shown).

Contraction Transient. Upon photolysis of c-ATP in the presence of Ca, the EPR transient is clearly biphasic (Figure 4). In the first phase of the transient, there is a rapid decrease in the signal intensity, corresponding to an essentially complete depopulation of the strong-binding structural state, just as in the absence of Ca. This is followed by a slower phase in which approximately half of the amplitude recovers as the system approaches the steady state of ATP hydrolysis. The mean recovery in six trials was 38 ± 8%, in agreement with the steady-state value of 34% (*1*, *5*). The exponential fit gives a τ_1 of 0.026 ± 0.007 s^{-1} ($1/\tau_1 = 38.5 \pm 8.2$ s^{-1}) for the rapid initial (falling) phase and a τ_2 of 0.12 ± 0.03 s^{-1} ($1/\tau_2 = 8.3 \pm 1.9$ s^{-1}) for the slower (rising) recovery phase. Presumably, the rapid phase corresponds to ATP binding and detachment from actin (resulting in net backward rotation of the lever arm on one of two heads in each myosin dimer), and the slower phase corresponds to the forward rotation of the lever arm in a fraction of myosin molecules, approaching a steady-state distribution in which approximately one-third of the myosin molecules (one-sixth of the heads, since the binding is probably single-headed) are in strong-binding states (*5*).

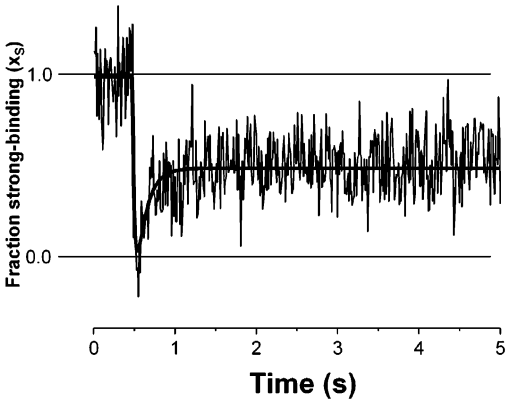

FIGURE 4: Transient rotation of spin-labeled RLC, induced by photolysis of caged ATP in the presence of Ca. The average of nine EPR transients is superimposed on the two-exponential fit.

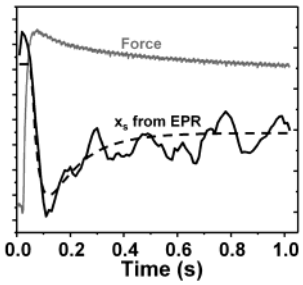

FIGURE 5: Transient force generation (gray, isometric force) and EPR (black, from Figure 4) following photolysis of caged ATP in the presence of Ca.

Upon release of ATP in the presence of Ca, force is generated rapidly (Figure 5). Surprisingly, maximal force is achieved prior to the complete redistribution of structural states as monitored by the spectral changes in M2. An exponential fit to the rate of force development yields a τ_{1force} of 0.0110 ± 0.0002 s^{-1} ($1/\tau_{1force} = 91 \pm 2$ s^{-1}), in close agreement with previous measurements using c-ATP, which determined the rate to be at least 41 s^{-1} (*22*). The force transient then shows a slow decline τ_{2force} of 0.240 ± 0.004 s^{-1} ($1/\tau_{2force} = 4.2 \pm 0.1$ s^{-1}).

Kinetic Modeling of Contraction Transients. The EPR transient in contraction (Figure 4) was fit to the kinetic model defined by Scheme 1. The kinetic simulation yielded the time-dependent concentration of each of the intermediates in Scheme 1. This allowed us to calculate the EPR observable $x_{S(t)}$, which is the molar fraction of myosin molecules in the strong-binding states (AM and AM·ADP). Rate constants were varied to minimize the χ^2 between the simulated and observed values of $x_S(t)$. The fit was constrained as indicated in Table 1, based on rate constants from the literature for scallop myosin, when possible, and rabbit myosin when scallop values were unavailable. Table 1 shows a comparison of the rate constants determined by the fitting procedure with known rate constants from the literature. Figure 6 shows the result of the best fit.

DISCUSSION

One of the main questions this paper seeks to address is how the structural transitions detected by EPR compare to known rates of the myosin biochemical cycle. Scheme 2

Table 1: Comparison of Literature Rate Constants and Those Determined from a Kinetic Fit of EPR Data[a] to Scheme 1

rate constant	constraints (min, max)	rate constant from the fit	literature value	muscle source	ref
k_{+1}	fixed	not applicable	118 s^{-1}	not applicable	*23*
k_{+2}	1.0×10^5 M^{-1} s^{-1}, 3.0×10^6 M^{-1} s^{-1}	2.0×10^5 M^{-1} $s^{-1} \pm 0.5$	1.6×10^6 M^{-1} s^{-1}	scallop	*24*
k_{-2}	fixed	0	~0	rabbit	*25*
k_{+3}	1 s^{-1}, 10 s^{-1}	4.5 ± 1.6 s^{-1}	30 s^{-1}	rabbit	*26*
k_{-3}	10 s^{-1}, 40 s^{-1}	37 ± 9 s^{-1}	20 s^{-1}	rabbit	*27*
k_{+4}	250 s^{-1}, 650 s^{-1}	480 ± 80 s^{-1}	300s $^{-1}$	rabbit	*26*
k_{-4}	1.0×10^5 M^{-1} s^{-1}, 2.0×10^5 M^{-1} s^{-1}	1.8×10^5 M^{-1} $s^{-1} \pm 0.4$	2.2×10^5 M^{-1} s^{-1}	rabbit	*26*
k_{+5}	0.5 s^{-1}, 10 s^{-1}	8.8 ± 2.1 s^{-1}	6 s^{-1}	scallop	*28*
k_{-5}	1.0×10^6 M^{-1} s^{-1}, 4.0×10^6 M^{-1} s^{-1}	2.7×10^6 M^{-1} $s^{-1} \pm 0.7$	2.1×10^6 M^{-1} s^{-1}	scallop	*24*

[a] Uncertainties are the standard error of the mean from six trials.

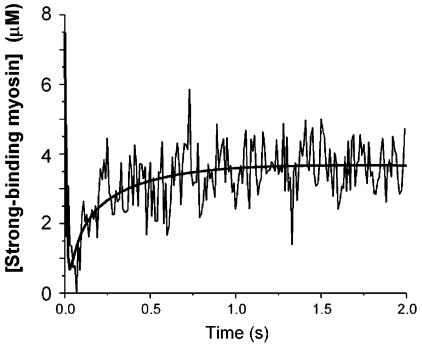

FIGURE 6: Kinetic modeling fit to EPR contraction transient data (Figure 4). The fit function is the fraction of myosin molecules in strong-binding states (AM and AM·ADP), based on Scheme 1.

Scheme 2

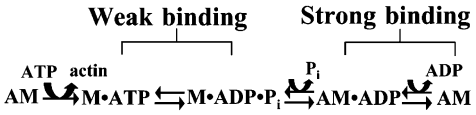

illustrates the basic actomyosin ATPase cycle, emphasizing that the biochemical reactions modulate actin−myosin affinity between weak- and strong-binding states. The transition from weak to strong binding occurs with phosphate release and has been postulated to be the force-generating step (*8*). Our previous steady-state EPR studies were the first to directly correlate a discrete lever arm rotation with strong actin binding, P_i release, and force generation in muscle (*1*, *6*, *29*). Although these previous studies provide significant insights into the mechanochemical relationships in muscle that exist after a steady state is reached, they do not define the relationships between muscle force, myosin structure, and biochemistry in the transient phase that leads to the steady state. As demonstrated in this paper, these transient relationships provide surprising new insights into the mechanisms of muscle force generation.

Transient Lever Arm Rotations. Following the photolysis of c-ATP, we observe (Figures 3 and 4) a rapid decrease in the EPR signal, corresponding to a reversal of the lever arm rotation (M1 → M2, $1/\tau_1 = 38.5$ s^{-1} with Ca and $1/\tau_1 = 37$ s^{-1} without Ca). Because this lever arm reversal is thought to be the result of the relaxation of a myosin dimer within the M·T state (*6*), we conclude that τ_1 is the time it takes for a myosin dimer to detach from actin upon ATP binding and relax to its splayed configuration (*12*, *13*). This fast falling phase is followed by a slower rising phase in the EPR transient, which corresponds to a forward lever arm rotation (the M2 → M1 working step, $1/\tau_2 = 8.3$ s^{-1} with Ca and $1/\tau_2 = 2.4$ s^{-1} without Ca). (The lever arm rotation rate refers to the inverse frequency of a relatively discrete lever arm rotation, not an angular velocity of the lever arm.) This slow phase is observed both in the presence and in the absence of Ca, where the small amplitude for this phase in the absence of Ca probably results from partial constitutive activation due to incomplete light-chain exchange. Since an ATP-regenerating solution is being employed, it is unlikely that the slow phase is due to depletion of ATP.

Kinetic Model of the EPR Contraction Transient. The fit to the EPR spectral transient shown in Figure 6 was obtained using a standard kinetic analysis of the actomyosin ATPase cycle shown in Scheme 1, giving the rate constants shown in Table 1. Using the reverse lever arm rotation as our spectroscopic signature, the second-order rate constant we obtained for ATP-induced actin−myosin dissociation ($k_{+2} = 2.0 \times 10^5$ M^{-1} s^{-1}) is lower than that measured in solution for the ATP-induced dissociation of scallop S1 from actin [$k = 1.6 \times 10^6$ M^{-1} s^{-1} (*24*)]. Presumably, this is because we measure an additional structural relaxation that follows the detachment step measured in solution. The forward and reverse hydrolysis rates in scallop muscle are unknown, but the rates from the fit are realistic. The forward hydrolysis rate is much slower relative to the reverse rate than the measured rates of hydrolysis in rabbit fibers (Table 1), suggesting that the predominant weak-binding state is the prehydrolysis state, A·M·ATP. The turnover number predicted by the fit is 4 s^{-1}, which is comparable to the measured turnover number from fibers of this preparation [7.8 s^{-1} (*30*)].

The kinetic model that we used to fit our EPR transients employs standard enzyme kinetics methods to generate the best fit to the data. However, our kinetic model does not take into consideration the effects of force on actin−myosin ATPase kinetics. Upon comparison of our EPR transients with muscle force transients, it appears that describing the interplay between mechanics and kinetics is critical for explaining the molecular basis for force transients in muscle.

Transient Force Generation. Force transients following the photolysis of c-ATP in the presence of Ca in scallop muscle show an initial fast phase of force development followed by a slow decline in force. The two phases seen in our mechanical transients have rates ($1/\tau_{1force} = 91$ s^{-1} and $1/\tau_{2force} = 4.2$ s^{-1}) similar to those of the two phases in our simultaneously measured EPR transients (Figure 5). Whereas skeletal muscle fiber force transients show an initial decline in force after release of cATP (*31*), such a decline was not previously described for scallop muscle force transients (*22*) and is not a prominent feature of our mechanical transients. We speculate that this difference is due to the difference in regulation between the two muscle types (see the model

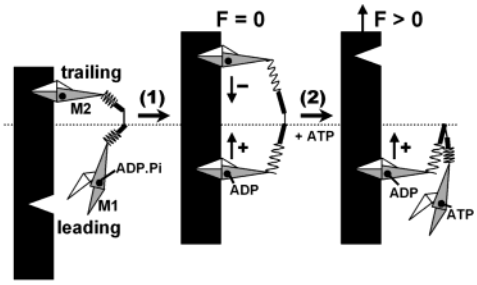

FIGURE 7: Model consistent with EPR and force transients. Actin is depicted as a black block, and compliant elements within myosin are depicted as springs. Before ATP release, negative and positive strains are balanced within the myosin molecule (middle), but upon ATP release, the detachment of the negatively strained head results in positive external force (right).

section below). On the basis of the above discussion of the EPR transients, we would have predicted that the fast phase of the force transient, corresponding to the ATP-induced actin−myosin detachment, would involve a decrease in force and that the slow phase of the force transient, corresponding to the M2 → M1 working step, would involve a force increase. Instead, we observe just the opposite (Figures 3−5). The lever arm reversal associated with actin−myosin dissociation correlates with a rapid increase in force, whereas the forward lever arm rotation associated with actin−myosin binding (thought to generate force) corresponds to a decrease in force. These surprising results can be explained with a simple model that involves balanced internal forces within rigor muscle, strain-dependent ADP affinities, and a steady-state distribution of states that is determined by muscle force.

Model for the Rapid Generation of Force Associated with ATP-Induced Actin−Myosin Dissociation. Figure 7 illustrates a model that can explain the rapid force increase that coincides roughly with the M2 → M1 EPR transient and precedes the M1 → M2 EPR transient (Figure 5). Step 1 shows the process that leads to the rigor state and precedes the photolysis of ATP: with the trailing head already strongly attached in the M2 state (Figure 7, left), the leading head binds to actin and undergoes its working step (M1 → M2 transition). This step results in both heads being bound strongly to actin, in the M2 orientation, at the expense of internal strain (Figure 7, middle). We observe that the rigor head orientation (M2) is unaffected by strain, confirming previous results (*32*), and so in Figure 7 we illustrate molecular strain localized to a region other than the light-chain domain.

Since force is adjusted to zero in rigor (Figure 7, middle) by the experimenter, negative strain in the trailing head must be balanced by positive strain in the leading head. These forces could be intramolecular (balanced within individual myosin dimers, as depicted) or intermolecular (balanced among myosin heads). At this point, ADP is bound to most heads, but we propose that ADP affinity is greater for the positively strained heads. Therefore, upon ATP release (Figure 7, step 2), ATP binding and detachment is more likely to occur first on the negatively strained head, resulting in the generation of positive force (Figure 7, right). According to this model, the rapid force development observed following the photolysis of c-ATP is the result of positively strained internal cross-bridge forces adding to the external muscle force when the balancing negatively strained cross-bridges detach from actin. On the basis of observed force transients in smooth muscle following the photolysis of c-ATP, a similar conclusion was reached (*33*). Here this hypothesis is bolstered by a direct correlation between rapid force generation and cross-bridge detachment.

An alternative point of view is that the rapid phase corresponds to force generation by weak binding cross-bridges. However, our EPR studies (*1*, *6*, *29*) and single-molecule mechanics studies of myosin (*34*) indicate that weak-binding cross-bridges cannot generate significant forces.

Interestingly, rapid force generation associated with actin−myosin detachment appears to be most pronounced in thick filament-regulated muscle such as scallop muscle, which suggests that it is related to the mechanism of thick filament regulation. For example, assuming that the aforementioned internal strain is intramolecular (within a myosin dimer), it may be that calcium binding to (in the case of molluscan muscle) or phosphorylation of (in the case of smooth muscle) the RLC makes the dimer more pliant. This would make it easier for the trailing head of a dimer to bind to an actin filament when the leading head is already bound, effectively increasing the rate of actin−myosin binding. This potential mechanism for thick filament regulation is supported by our observation that the rapid force transient upon addition of ATP is minimized in muscle fibers that have been constitutively activated through the selective removal of one light chain from myosin dimers (data not shown). As previously mentioned, skeletal muscle instead shows an initial drop in tension (*31*), suggesting that there are fewer negatively strained heads bound or that the actin−myosin detachment kinetics (e.g., ADP release or ATP binding) is less sensitive to strain.

Model for a Slow (Relative to Force Generation) Weak-to-Strong Binding Transition. EPR has shown that the forward lever arm rotation has been correlated with the weak-to-strong binding biochemical transition (M1 → M2) and force generation in steady-state muscle studies (*1*, *29*). However, in the transient studies reported in this paper, the forward lever arm rotation rate (8.33 s^{-1}) is slow relative to the rate of force development (91 s^{-1}). Here we discuss possible explanations for this observation.

Our data imply that cross-bridges can transiently generate a large average force per cross-bridge (in Figure 4, muscle force is near a maximum when the fraction of strong-binding heads is near its minimum) that cannot be sustained in the steady state (Figures 3−5). Thus, the approach to steady state involves a dynamic redistribution of both cross-bridge forces and biochemical states. For example, if the force generated by the initial transient is to be maintained as the steady state is approached, a decrease in the average force per cross-bridge must be compensated by an increase in the fraction of force-bearing strongly bound myosin heads. Thus, we suggest that the slow EPR transient, corresponding to a net shift from weak- to strong-binding states, reflects a compensatory redistribution of cross-bridge forces and biochemical states on approach to the steady state. In the end, as suggested by our previous studies of mechanochemical coupling in muscle (*14*, *29*), it is the binding energy for the weak-to-strong binding transition that determines the steady-state force, and the steady-state force in turn determines (in

a Boltzmann fashion) the steady-state distribution of myosin states. That is

$$[A{\cdot}M{\cdot}D]/[M{\cdot}D{\cdot}P_i] = A \exp[(-Fd)/(RT)]$$

where A and d are constants.

In our experiments, it appears that the redistribution of cross-bridge forces and states on approach to the steady state actually involves a slight dissipation of force (Figures 3−5), and (consistent with the above equation) the shift in the distribution of states from M·D·P_i to A·M·D follows this decrease in muscle force. Thus, we suggest that τ_2 is the time it takes to reach a steady state after photolysis of c-ATP, and that this relaxation time is influenced by the force-dependent kinetics of the entire ATPase reaction.

A similarly slow (relative to force development) approach to the steady-state ATPase rate following the photolysis of c-ATP was previously demonstrated by He et al. in skeletal muscle (*35*). They interpreted this slow approach to a steady state as a redistribution of myosin molecules among force-bearing strongly bound states. However, in this paper, we show that the slow approach to steady state involves a net shift of myosin heads from weak- to strong-binding states. As discussed above, this requires a dynamic redistribution of cross-bridge forces as well as a redistribution of cross-bridge biochemical states.

Conclusions. The transient kinetics of the myosin lever arm rotation and its reversal yield two dramatic results. The fast phase of the EPR transient following photolysis of c-ATP corresponds to an axial rotation of the light-chain domain (a reverse lever arm rotation), which presumably occurs when the myosin dimer relaxes to its splayed configuration. This structural relaxation is critical for positioning the myosin head at an orientation that maximizes the force it can generate with the subsequent forward lever arm rotation. Surprisingly, we observe that rapid force development is closely associated with this actin−myosin detachment step, suggesting that ATP binds preferentially to negatively strained cross-bridges in rigor muscle and the force transient results from the positively strained cross-bridges that remain bound to actin. The slow phase of the EPR transient corresponds to a net lever arm rotation associated with the establishment of a steady-state distribution of weak- and strong-binding heads. Surprisingly, the rate of this lever arm transient is much slower than the rate of force development, suggesting that the approach to steady state involves a redistribution of cross-bridge forces as well as a redistribution of biochemical states. In general, this study implies that the kinetics of the actin−myosin ATPase reaction are significantly influenced by the forces that are generated, and that describing the complex interplay between cross-bridge mechanics and chemistry is critical for understanding the molecular basis for force-generating transients in muscle.

ACKNOWLEDGMENT

We thank Jack Surek and John Marchetti for development of fiber mounting and force measurement devices. We thank Jack Grinband for writing the LabView control program, for assistance with laser maintenance, and for helpful discussions. We thank Orion Rainwater and Cheryl Miller for care and maintenance of the scallops and Sarah Blakely for assistance with scallop fiber preparation. We thank Diane Lidke and Dawn Lowe for helpful discussions.

REFERENCES

1. Baker, J. E., Brust-Mascher, I., Ramachandran, S., LaConte, L. E., and Thomas, D. D. (1998) *Proc. Natl. Acad. Sci. U.S.A. 95*, 2944−2949.
2. Rayment, I., Holden, H. M., Whittaker, M., Yohn, C. B., Lorenz, M., Holmes, K. C., and Milligan, R. A. (1993) *Science 261*, 58−65.
3. Irving, M., St Claire Allen, T., Sabido-David, C., Craik, J. S., Brandmeier, B., Kendrick-Jones, J., Corrie, J. E., Trentham, D. R., and Goldman, Y. E. (1995) *Nature 375*, 688−691.
4. Uyeda, T. Q., Abramson, P. D., and Spudich, J. A. (1996) *Proc. Natl. Acad. Sci. U.S.A. 93*, 4459−4464.
5. Lidke, D. S., and Thomas, D. D. (2002) *Proc. Natl. Acad. Sci. U.S.A. 99*, 14801−14806.
6. Brust-Mascher, I., LaConte, L. E., Baker, J. E., and Thomas, D. D. (1999) *Biochemistry 38*, 12607−12613.
7. Lymn, R. W., and Taylor, E. W. (1971) *Biochemistry 10*, 4617−4624.
8. Eisenberg, E., and Hill, T. L. (1985) *Science 227*, 999−1006.
9. Dantzig, J. A., Higuchi, H., and Goldman, Y. E. (1998) *Methods Enzymol. 291*, 307−348.
10. Thomas, D. D., Ostap, E. M., Berger, C. L., Lewis, S. M., Fajer, P. G., and Mahaney, J. E. (1993) in *EMR of Paramagnetic Molecules* (Berliner, L. J., and Reuben, J., Eds.) pp 323−349, Plenum Press, New York.
11. Goldman, Y. E. (1987) *Annu. Rev. Physiol. 49*, 637−654.
12. Wray, J. S., Vibert, P. J., and Cohen, C. (1975) *Nature 257*, 561−564.
13. Vibert, P. (1992) *J. Mol. Biol. 223*, 661−671.
14. Baker, J. E., and Thomas, D. D. (2000) *J. Muscle Res. Cell Motil. 21*, 335−344.
15. Persechini, A., and Hartshorne, D. J. (1983) *Biochemistry 22*, 470−476.
16. Simmons, R. M., and Szent-Gyorgyi, A. G. (1980) *Nature 286*, 626−628.
17. Mendes, P. (1993) *Comput. Appl. Biosci. 9*, 563−571.
18. Mendes, P. (1997) *Trends Biochem. Sci. 22*, 361−363.
19. Mendes, P., and Kell, D. (1998) *Bioinformatics 14*, 869−883.
20. Cooke, R., Crowder, M. S., and Thomas, D. D. (1982) *Nature 300*, 776−778.
21. Palmer, R. E., Mulligan, I. P., Nunn, C., and Ashley, C. C. (1990) *Biochem. Biophys. Res. Commun. 168*, 295−300.
22. Lea, T. J., Fenton, M. J., Potter, J. D., and Ashley, C. C. (1990) *Biochim. Biophys. Acta 1034*, 186−194.
23. McCray, J. A., and Trentham, D. R. (1989) *Annu. Rev. Biophys. Biophys. Chem. 18*, 239−270.
24. Kurzawa-Goertz, S. E., Perreault-Micale, C. L., Trybus, K. M., Szent-Gyorgyi, A. G., and Geeves, M. A. (1998) *Biochemistry 37*, 7517−7525.
25. Hibberd, M. G., and Trentham, D. R. (1986) *Annu. Rev. Biophys. Biophys. Chem. 15*, 119−161.
26. Dantzig, J. A., Goldman, Y. E., Millar, N. C., Lacktis, J., and Homsher, E. (1992) *J. Physiol. 451*, 247−278.
27. Sleep, J. A. (1981) *Biochemistry 20*, 5043−5051.
28. Jackson, A. P., and Bagshaw, C. R. (1988) *Biochem. J. 251*, 515−526.
29. Baker, J. E., LaConte, L. E., Brust-Mascher, I. I., and Thomas, D. D. (1999) *Biophys. J. 77*, 2657−2664.
30. Ramachandran, S., and Thomas, D. D. (1999) *Biochemistry 38*, 9097−9104.
31. Goldman, Y. E., Hibberd, M. G., and Trentham, D. R. (1984) *J. Physiol. 354*, 605−624.
32. Zhao, L., Gollub, J., and Cooke, R. (1996) *Biochemistry 35*, 10158−10165.
33. Somlyo, A. V., Goldman, Y. E., Fujimori, T., Bond, M., Trentham, D. R., and Somlyo, A. P. (1988) *J. Gen. Physiol. 91*, 165−192.
34. Baker, J. E., Brosseau, C., Joel, P. B., and Warshaw, D. M. (2002) *Biophys. J. 82*, 2134−2147.
35. He, Z. H., Chillingworth, R. K., Brune, M., Corrie, J. E., Trentham, D. R., Webb, M. R., and Ferenczi, M. A. (1997) *J. Physiol. 501*, 125−148.

BI034288R